Ultrasonic measurement of the porosity and tortuosity of air-saturated random packings of beads

Zine El Abiddine Fellah, S Berger, W Lauriks, C Depollier, P Trompette, J Y Chapelon

Ultrasonic measurement of the porosity and tortuosity of air-saturated random packings of beads

Z. E. A. Fellah[a)]
National Institute of Health and Medical Research (INSERM U556), 151 cours Albert Thomas, 69424 Lyon Cedex 03, France

S. Berger and W. Lauriks
Laboratorium voor Akoestiek en Thermische Fysica, Katholieke Universiteit Leuven, Celestijnenlaan 200 D, B-3001 Heverlee, Belgium

C. Depollier
Laboratoire d'Acoustique de l'Université du Maine, UMR–CNRS 6613, Université du Maine, Avenue Olivier Messiaen 72085 Le Mans Cedex 09, France

P. Trompette and J. Y. Chapelon
National Institute of Health and Medical Research (INSERM U556), 151 cours Albert Thomas, 69424 Lyon Cedex 03, France

(Received 19 November 2002; accepted 14 March 2003)

In the pore space of packed grain material, transport properties are characterized by macroscopic parameters. Some of them, porosity and tortuosity, are measured for random packing of glass beads and compared with evaluations made during previous studies. A simple method for measuring porosity and tortuosity for air-saturated granular media is given. This method is based on a temporal model of the direct and inverse scattering problem for the propagation of transient ultrasonic waves in a homogeneous isotropic slab of porous material with a rigid frame. Viscous and thermal losses of the medium are described by temporal operators describing memory effects in a porous medium. Because of the high attenuation of acoustic waves in air-saturated packings of beads, the wave reflected by this medium is equivalent to the wave reflected by the first interface. Using this approximation, a simple relation between porosity, tortuosity, the angle of incidence, and the reflected wave is obtained. Porosity and tortuosity are thus measured via reflected waves in the porous medium at oblique incidence. Experimental and numerical validation results for this method are given for a sample of random packings of glass beads. © *2003 American Institute of Physics*.
[DOI: 10.1063/1.1572191]

I. INTRODUCTION

The ultrasonic characterization of porous materials saturated by air, such as granular materials,[1] fibrous or plastic foams is of great interest for a wide range of industrial applications. These materials are frequently used in the automobile and aeronautics industries as well as the building trade.

Disorder granular media, including bead packings, have been studied using different approaches.[2] A partial description of a granular medium at the macroscopic scale (over a large volume compared to grain size) can be produced by evaluating different macroscopic parameters, dependent only on the geometry of the granular structure. Some of them can be used to characterize sound propagation in air saturating the pore space, and, conversely, can be evaluated from acoustic measurements.

Attenborough[3] has suggested an elegant model for obtaining the acoustical properties of air-saturated granular media. Random bead packing is replaced by a system of parallel slits with a log–normal distribution for the semithickness. The macroscopic parameters relative to a similar model have been calculated by Lafarge *et al.*[4]

Allard *et al.*[5] characterize the random packing of glass beads by measuring macroscopic acoustic parameters. A prediction of surface impedance at normal incidence for a layer of glass beads is given.

Two important parameters used in theories of sound propagation in porous materials[1,3–13] are porosity and the tortuosity. Porosity is the relative fraction, by volume, of air contained within the material. Unlike other parameters involved in the description of different physical phenomena involved in the acoustic propagation of porous media at the high frequency range, such as tortuosity,[14] viscous characteristic length,[9] and thermal characteristic length,[15] or at the low frequency range, such as flow resistivity[15] and thermal permeability,[4] porosity is a key parameter playing an important part in propagation at all frequencies. As such, in studies of the acoustic properties of porous materials, it is highly desirable to be able to measure this parameter.

Beranek[16] described an apparatus (porosimeter) for measuring the porosity of porous materials. This device was based on the equation of state for ideal gases at constant temperature (i.e., Boyle's law). Measuring the change in air

a)Electronic mail: fellah@lyonl.inserm.fr

pressure, for a known change in volume of the chamber containing the sample, allows porosity to be determined. In the Beranek apparatus, both pressure change and volume change are monitored by using a U-shaped fluid-filled manometer. An alternative technique for measuring porosity is a dynamic method suggested by Leonard.[17] Techniques that use water rather than air as the pore-filling fluid, are common in geophysical studies.[18,19] Mercury has been used as the pore-filling fluid in other applications.[20] However, for many materials, the introduction of liquids into the material is not appropriate. Recently, a similar device to that used by Beranek, with an electronic pressure transducer, has been introduced by Champoux *et al.*,[21] where very small changes of pressure can be measured accurately, and the output recorded on a computer.

Tortuosity α_∞, named the structure factor k_s by Zwikker and Kosten[14] or the parameter q^2 by Attenborough,[13] is an important parameter which is used in describing inertial interaction between fluid and structure in porous material at high frequency range. In the case of cylindrical pores at an angle ϑ to the direction of propagation, $\alpha_\infty = 1/\cos^2 \vartheta$. Tortuosity can be evaluated by electrical measurements,[19] or by using a superfluid ^{4}He as the pore fluid.[9] It can also be evaluated using acoustic techniques such as ultrasonic measurement of transmitted waves.[7,8,23,24]

In this work, we present a simple method of measuring porosity and tortuosity by measuring the acoustic wave reflected by a slab of porous material at oblique incidence. This method is based on a temporal model of the direct and inverse scattering problem for the propagation of transient ultrasonic waves in a homogeneous isotropic slab of porous material with a rigid frame, initially introduced by the authors in Refs. 6–8. The viscous and thermal losses of the medium are described by Johnson *et al.*[9] and Allard[10] model modified by a fractional calculus based method for use in the time domain. Reflection and transmission scattering operators for a slab of porous material are derived for an oblique incidence and the responses of the medium to an incident acoustic pulse are obtained.

The outline of this article is as follows. In Sec. II a time domain model is given, the connection between fractional derivatives and wave propagation in rigid porous media at the high frequency range is established, and the basic equations are written in the time domain. Section III is devoted to the direct problem and general expression of the acoustic field inside the porous medium, expression of reflection and transmission kernels in the time domain at oblique incidence are calculated and numerical results given. Finally, in Sec. IV an experimental validation using ultrasonic measurement is performed for random packings of glass beads. Porosity and tortuosity are measured via reflected waves for different incidence angles.

II. MODEL

In the acoustics of porous materials, a distinction can be made between two situations depending on whether the frame is moving or not. In the first case, the wave dynamics due to coupling between the solid frame and the fluid are clearly described by the Biot theory.[11,12] In air-saturated porous media the structure is generally motionless and the waves propagate only in the fluid. This case is described by the equivalent fluid model which is a particular case in the Biot model, in which the interactions between fluid and structure are taken into account for two frequency response factors: dynamic tortuosity of the medium $\alpha(\omega)$ given by Johnson *et al.*[9] and dynamic compressibility of air in the porous material $\beta(\omega)$ given by Allard.[10] In the frequency domain, these factors multiply fluid density and compressibility respectively and represent the deviation from fluid behavior in free space as the frequency increases. In the time domain, they act as operators and in the asymptotic domain (high frequency approximation) their expressions are given[6–8] by

$$\tilde{\alpha}(t) = \alpha_\infty \left[\delta(t) + \frac{2}{\Lambda} \left(\frac{\eta}{\pi \rho_f} \right)^{1/2} t^{-1/2} \right], \tag{1}$$

$$\tilde{\beta}(t) = \left[\delta(t) + \frac{2(\gamma - 1)}{\Lambda'} \left(\frac{\eta}{\pi \mathrm{Pr} \rho_f} \right)^{1/2} t^{-1/2} \right]. \tag{2}$$

In Eqs. (1) and (2), $\delta(t)$ is the Dirac function; Pr is the Prandtl number; η and ρ_f the fluid viscosity and fluid density, respectively; and γ is the adiabatic constant. The relevant physical parameters of the model are the tortuosity of the medium α_∞ initially introduced by Zwikker and Kosten[14] and the viscous and thermal characteristic lengths Λ and Λ' introduced by Johnson *et al.*[9] and Allard.[10] In this model, the time convolution of $t^{-1/2}$ with a function is interpreted as a semi derivative operator following definition of the fractional derivative of order ν given in Samko and Coll,[22]

$$D^\nu [x(t)] = \frac{1}{\Gamma(-\nu)} \int_0^t (t-u)^{-\nu-1} x(u) du, \tag{3}$$

where $\Gamma(x)$ is the gamma function.

In this framework, the basic equations of our model can be expressed as follows:

$$\rho_f \tilde{\alpha}(t) * \frac{\partial v_i}{\partial t} = -\nabla_i p \quad \text{and} \quad \frac{\tilde{\beta}(t)}{K_a} * \frac{\partial p}{\partial t} = -\nabla v, \tag{4}$$

where* denotes the time convolution operation, p is acoustic pressure, v is particle velocity, and K_a is the bulk modulus of air. The first equation is the Euler equation, the second is a constitutive equation obtained from the equation of mass conservation associated with the behavior (or adiabatic) equation.

For a wave propagating at oblique incidence in plane (xoz) at an angle θ along the x axis, these equations become

$$\rho_f \alpha_\infty \frac{\partial v_x(x,z,t)}{\partial t} + \frac{2\rho_f \alpha_\infty}{\Lambda} \left(\frac{\eta}{\pi \rho_f} \right)^{1/2} \int_0^t \frac{\partial v(x,z,t')/\partial t'}{\sqrt{t-t'}} dt' = -\frac{\partial p(x,z,t)}{\partial x},$$

$$\rho_f \alpha_\infty \frac{\partial v_z(x,z,t)}{\partial t} + \frac{2\rho_f \alpha_\infty}{\Lambda}\left(\frac{\eta}{\pi\rho_f}\right)^{1/2}\int_0^t \frac{\partial v(x,z,t')/\partial t'}{\sqrt{t-t'}}dt' = -\frac{\partial p(x,z,t)}{\partial z}, \tag{5}$$

$$\frac{1}{K_a}\frac{\partial p(x,z,t)}{\partial t} + \frac{2(\gamma-1)}{K_a\Lambda'}\left(\frac{\eta}{\pi\rho_f \mathrm{Pr}}\right)^{1/2}\int_0^t \frac{\partial p(x,z,t')/\partial t'}{\sqrt{t-t'}}dt' = -\frac{\partial v(x,z,t)}{\partial x} - \frac{\partial v(x,z,t)}{\partial z},$$

where v_x, v_z are the components of particle velocity along the ox and oz axes.

In theses equations, the convolutions express the dispersive nature of porous material. They take into account memory effects due to the fact that the medium's response to wave excitation is not instantaneous but needs more time to take effect. The retarding force is no longer proportional to the time derivative of the acoustic velocity but is found to be proportional to the fractional derivative of about $\frac{1}{2}$ of this quantity. This occurs because the volume of fluid participating in the motion is not the same for all motion, as it is for a fully developed steady flow. The phenomenon may be understood by considering such a volume of fluid in a pore to be in harmonic motion. At high frequencies, only a thin layer of fluid is excited so that average shear stress is high. At a lower frequency, the same amplitude of fluid motion allows a thicker layer of fluid to take part in the motion and consequently the shear stress is lower. The penetration distance of viscous forces and therefore excitation of the fluid depends on frequency. In the time domain, such dependence is associated with a fractional derivative.

III. DIRECT PROBLEM

The direct scattering problem is that of determining the scattered field, as well as the internal field, that arises when a known incident field impinges on porous material with known physical properties. To compute the solution of the direct problem, it is necessary to know the reflection and/or transmission scattering operators which depend on the Green[7] function of the porous medium. In that case, the reflected field is given by the convolution of the reflection operator with the incident field and the transmitted field is given by the convolution of the transmission operator by the incident field.

Consider a homogeneous slab of porous material which occupies region $0 \leqslant x \leqslant L$. The problem geometry is shown in Fig. 1. This medium is assumed to be isotropic and to have a rigid frame. A short sound pulse impinges at oblique incidence on the medium from the left. It gives rise to an acoustic pressure field $p(x,t)$ and an acoustic velocity field $v(x,t)$ within the material, which satisfies the propagation equation[6] along the x axis:

$$\frac{\partial^2 p(x,t)}{\partial x^2} - A\frac{\partial^2 p(x,t)}{\partial t^2} - B\frac{\partial^{3/2} p(x,t)}{\partial t^{3/2}} - C\frac{\partial p(x,t)}{\partial t} = 0, \tag{6}$$

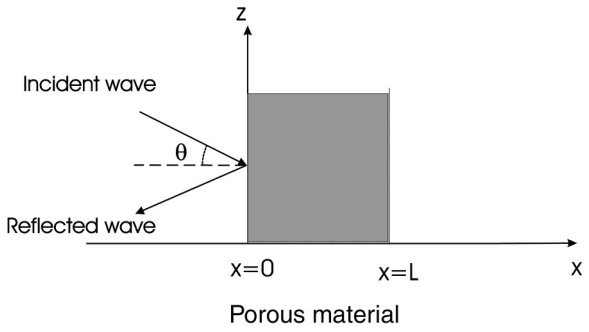

FIG. 1. Problem geometry.

where coefficients A, B, and C are constants, respectively, given by

$$A = \frac{1}{c_0^2}(\alpha_\infty - \sin^2\theta),$$

$$B = \frac{2\alpha_\infty}{K_a}\sqrt{\frac{\rho_f \eta}{\pi}}\left(\frac{1}{\Lambda} + \frac{\gamma-1}{\sqrt{\mathrm{Pr}}\Lambda'}\right),$$

$$C = \frac{4\alpha_\infty(\gamma-1)\eta}{K_a \Lambda\Lambda'\sqrt{\mathrm{Pr}}}. \tag{7}$$

The first is related to projected wave velocity along the x-axis $c = c_0/\sqrt{\alpha_\infty - \sin^2\theta}$. The other coefficients are essentially dependent on the characteristic lengths Λ and Λ' and express the viscous and thermal interactions between the fluid and the structure. Constant B governs the signal spreading while C is responsible for wave attenuation. Obviously, knowledge of these three coefficients means that parameters α_∞, Λ, and Λ' can be determined. One way of solving Eq. (6) with suitable initial and boundary conditions is by using the Laplace transform. The approach is quite simple although the inverse Laplace transform require tedious calculus.[7] A suitable setting for introducing the time domain solution of the modified wave propagation Eq. (6) is given in the following model.

To derive reflection and transmission scattering operators, it is assumed that the pressure field and flow velocity are continuous at the boundary of the material

$$\begin{aligned} &p(0^+,t) = p(0^-,t), \quad p(L^-,t) = p(L^+,t), \\ &v(0^-,t) = \phi v(0^+,t), \quad v(L^+,t) = \phi v(L^-,t), \end{aligned} \tag{8}$$

where ϕ is the porosity of the medium and $\pm$ superscript denotes the limit from left and right, respectively. Initial conditions are given by

$$p(x,t)\big|_{t=0} = 0 \quad \left.\frac{\partial p}{\partial t}\right|_{t=0} = 0, \tag{9}$$

which means that the medium is idle for $t=0$.

If the incident sound wave is launched in region $x \leqslant 0$, then the general solution of Eq. (6) in the region to the left of the material is the sum of the incident and reflected fields:

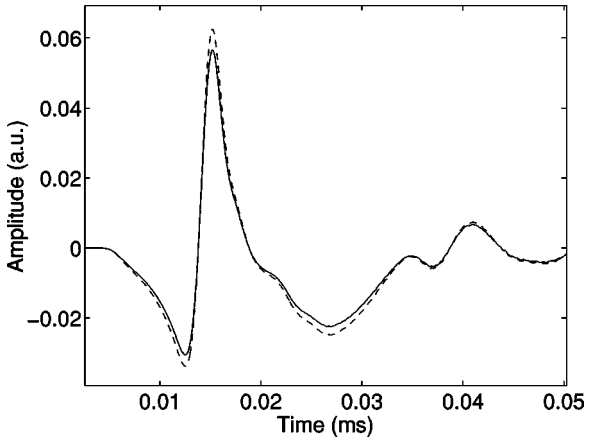

FIG. 2. Transmitted simulated signals for $\phi=0.45$ (solid line) and $\phi=0.58$ (dashed line).

$$p_1(x,t)=p^i\left(t-\frac{x\cos\theta}{c_0}\right)+p^r\left(t+\frac{x\cos\theta}{c_0}\right),\quad x<0, \tag{10}$$

here, $p_1(x,t)$ is the field in region $x<0$, p^i and p^r denotes the incident and reflected fields, respectively. In addition, a transmitted field is produced in the region to the right of the material. This takes the form

$$p_3(x,t)=p^t\left(t-\frac{L}{c}-\frac{(x-L)\cos\theta}{c_0}\right),\quad x>L, \tag{11}$$

where $p_3(x,t)$ is the field in region $x>L$ and p^t is the transmitted field .

Incident and scattered fields are related by the scattering operators (i.e., reflection and transmission operators) for the material. These are integral operators represented by

$$\begin{aligned} p^r(x,t)&=\int_0^t\tilde{R}(\tau)p^i\left(t-\tau+\frac{x}{c_0}\right)d\tau\\ &=\tilde{R}(t)*p^i(t)*\delta\left(t+\frac{x\cos\theta}{c_0}\right),\\ p^t(x,t)&=\int_0^t\tilde{T}(\tau)p^i\left(t-\tau-\frac{L}{c}-\frac{(x-L)}{c_0}\right)d\tau\\ &=\tilde{T}(t)*p^i(t)*\delta\left(t-\frac{L}{c}-\frac{(x-L)\cos\theta}{c_0}\right). \end{aligned} \tag{12}$$

In Eqs. (12) functions $\tilde{R}$ and $\tilde{T}$ are the reflection and transmission kernels, respectively, for the incidence of waves from the left. Note that the lower limit of integration in Eq. (12) is set to 0, which is equivalent to assuming that the incident wave front first impinges on the material at $t=0$. The scattering operators given in Eqs. (12) are independent of the incident field used in the scattering experiment and depend only on the properties of the materials. Using the Eqs. (4), (6), (8), and (12) and Laplace transform calculus, we can derive the reflection and transmission scattering operators given by

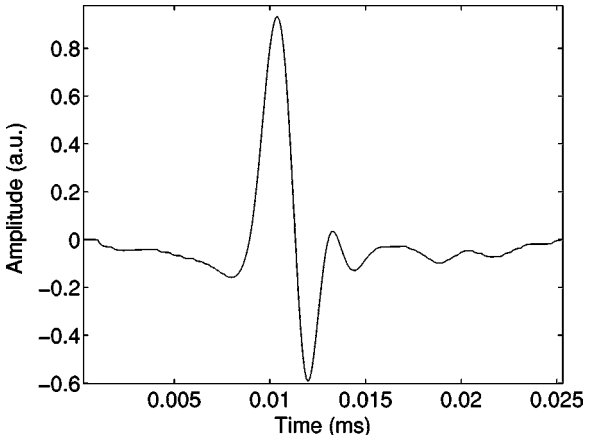

FIG. 3. Input signal.

$$\begin{aligned} \tilde{R}(t)=&\left(\frac{\alpha_\infty\cos\theta-\phi\sqrt{\alpha_\infty-\sin^2\theta}}{\alpha_\infty\cos\theta+\phi\sqrt{\alpha_\infty-\sin^2\theta}}\right)\\ &\times\sum_{n\geqslant 0}\left(\frac{\alpha_\infty\cos\theta-\phi\sqrt{\alpha_\infty-\sin^2\theta}}{\alpha_\infty\cos\theta+\phi\sqrt{\alpha_\infty-\sin^2\theta}}\right)^{2n}\\ &\times\left[F\left(t,2n\frac{L}{c}\right)-F\left(t,(2n+2)\frac{L}{c}\right)\right], \end{aligned} \tag{13}$$

$$\begin{aligned} \tilde{T}(t)=&\frac{4\phi\cos\theta\sqrt{\alpha_\infty-\sin^2\theta}}{\left(\sqrt{\alpha_\infty}\cos\theta+\phi\sqrt{1-\dfrac{\sin^2\theta}{\alpha_\infty}}\right)^2}\\ &\times\sum_{n\geqslant 0}\left(\frac{\alpha_\infty\cos\theta-\phi\sqrt{\alpha_\infty-\sin^2\theta}}{\alpha_\infty\cos\theta+\phi\sqrt{\alpha_\infty-\sin^2\theta}}\right)^{2n}\\ &\times F\left(t+\frac{L}{c_0},(2n+1)\frac{L}{c}\right), \end{aligned} \tag{14}$$

where $c=c_0/\sqrt{\alpha_\infty-\sin^2\theta}$. These expressions take into account n-multiple reflections in the material. For a positive constant k, $F(t,k)$ is the Green function of porous material given in Ref. 7 (the Appendix).

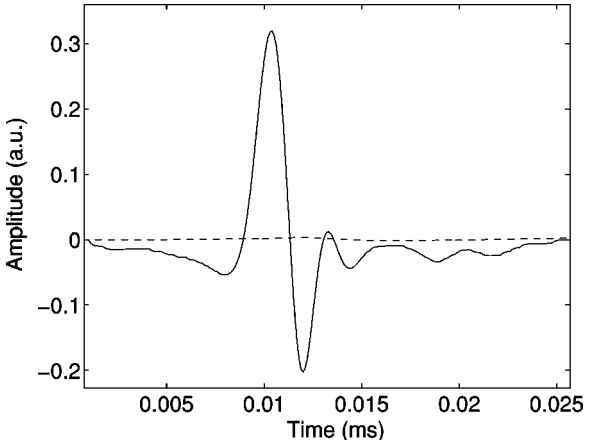

FIG. 4. Numerical simulations of reflection contributions $r(t)$ (solid line) and $\Re(t)$ (dashed line).

In most cases, for air-saturated porous materials, multiple reflection effects are negligible because of the high attenuation of sound waves in this kind of medium. So, by taking into account only the reflections at the $x=0$ and $x=L$ interfaces, the transmission kernel is given by

$$\tilde{T}(t)=\frac{4\phi\cos\theta\sqrt{\alpha_\infty-\sin^2\theta}}{\left(\sqrt{\alpha_\infty}\cos\theta+\phi\sqrt{1-\frac{\sin^2\theta}{\alpha_\infty}}\right)^2}F\left(t+\frac{L}{c},\frac{L}{c}\right), \tag{15}$$

and the reflection kernel by

$$\tilde{R}(t)=r(t)+\Re(t), \tag{16}$$

with

$$r(t)=\left(\frac{\alpha_\infty\cos\theta-\phi\sqrt{\alpha_\infty-\sin^2\theta}}{\alpha_\infty\cos\theta+\phi\sqrt{\alpha_\infty-\sin^2\theta}}\right), \tag{17}$$

and

$$\Re(t)=-\frac{4\phi\cos\theta\sqrt{\alpha_\infty-\sin^2\theta}\left(\sqrt{\alpha_\infty}\cos\theta-\phi\sqrt{1-\frac{\sin^2\theta}{\alpha_\infty}}\right)}{\left(\sqrt{\alpha_\infty}\cos\theta+\phi\sqrt{1-\frac{\sin^2\theta}{\alpha_\infty}}\right)}F\left(t,\frac{2L}{c}\right), \tag{18}$$

in the case of a semi-infinite medium when $L\to\infty$; $F(t,2L/c)\to 0$ and $\tilde{R}(t)\to r(t)$ (the Appendix). This means that $r(t)$ is equivalent to the reflection at interface $x=0$ and that $\Re(t)$ is equivalent to reflection at interface $x=L$, which is the bulk contribution to the reflection. The part of the wave corresponding to $r(t)$ is not subject to dispersion but is simply multiplied by the factor

$$\left(\frac{\alpha_\infty\cos\theta-\phi\sqrt{\alpha_\infty-\sin^2\theta}}{\alpha_\infty\cos\theta+\phi\sqrt{\alpha_\infty-\sin^2\theta}}\right).$$

This shows that although tortuosity is a bulk parameter, it may be evaluated from the wave reflected at the first interface when the porosity is known and vice versa. Although generally speaking it is easy to evaluate tortuosity from transmitted waves,[3,4,20,21] this is not the case for porosity because of its weak sensitivity in the transmitted mode.

Figure 2 shows two simulated transmitted signals for a sample of random packings of glass beads M1 at normal incidence, the first (solid line) corresponding to a porosity value of $\phi 1=0.45$ and the second (dashed line) to $\phi 2=0.58$. The parameters used in the simulation are: diameter 0.5 mm, thickness 0.5 cm, $\alpha_\infty=1.4$, $\Lambda=20$ μm, and $\Lambda'=60$ μm and were determined using conventional methods.[7,8,23,24] A slight difference can be seen between the two curves for a 30% difference in porosity values, due to the dispersion phenomenon governed by viscous, thermal and inertial effects provided by α_∞, Λ and Λ' and plays a more important role in the Green function $F(t,k)$ than ϕ. The input signal used in the simulation is given in Fig. 3.

Figure 4 shows the two contributions to reflection: $r(t)$ and $\Re(t)$ for sample M1 having porosity $\phi=0.45$. The contribution of $\Re(t)$ to reflection is negligible when compared to the contribution of $r(t)$. In Fig. 5 we show by numerical simulation, the difference between the reflected wave at the first interface, and the total reflected wave for the sample M1

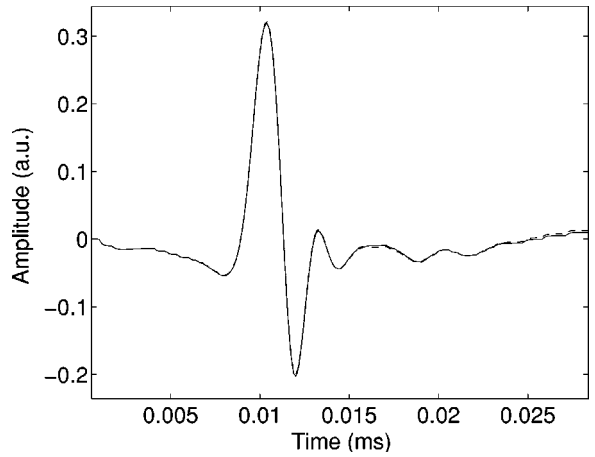

FIG. 5. Reflected wave at the interface $x=0$ (solid line) and total reflected wave (dashed line).

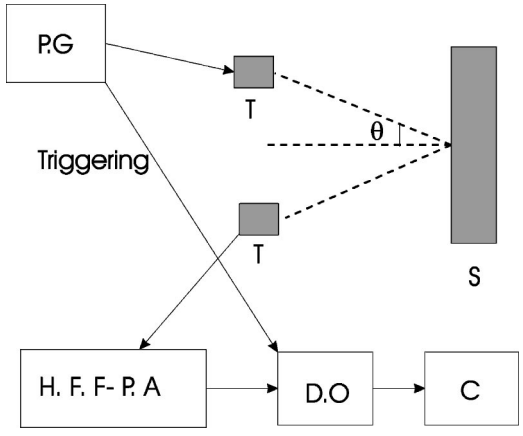

FIG. 6. Experimental setup for ultrasonic measurements in reflected mode. P.G: pulse generator, H. F. F-P. A: high frequency filtering-preamplifier, D.O: digital oscilloscope, C: computer, T: transducer, and S: sample.

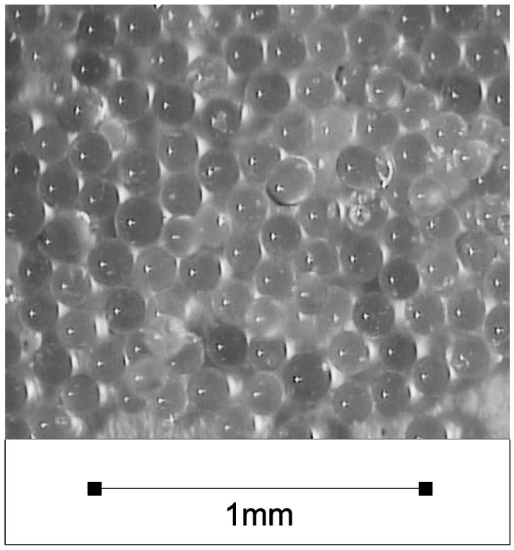

FIG. 7. Sample of random packings of glass beads M2.

having porosity $\phi=0.45$. The difference between the two curves is negligible. This means that the wave reflected by the sample may be approximated by the reflected wave at the first interface $r(t)$ with a high level of accuracy.

IV. ULTRASONIC MEASUREMENT

In this section, we measure tortuosity and porosity knowing the reflection coefficient at the first interface for different values of angle of incidence θ. Expression of the reflection coefficient at the first interface is given by

$$r(t)=\frac{\alpha_\infty \cos\theta-\phi\sqrt{\alpha_\infty-\sin^2\theta}}{\alpha_\infty \cos\theta+\phi\sqrt{\alpha_\infty-\sin^2\theta}}. \tag{19}$$

For two values of the angle of incidence θ_1 and θ_2, it is easy to calculate the expression of the tortuosity function for reflection coefficients $r1$ and $r2$ corresponding, respectively, to angles θ_1 and θ_2:

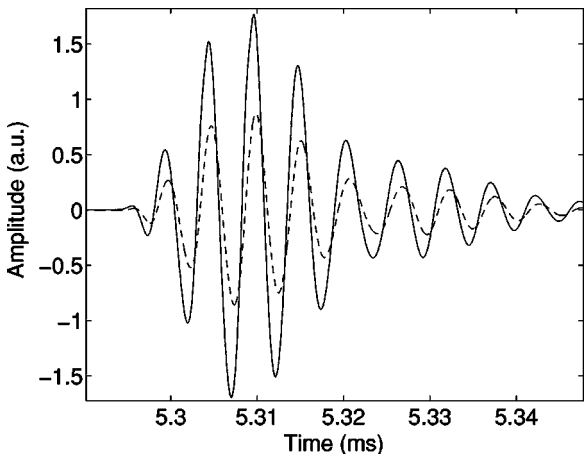

FIG. 8. Experimental incident signal (solid line) and experimental reflected signal (dashed line) for $\theta=25°$.

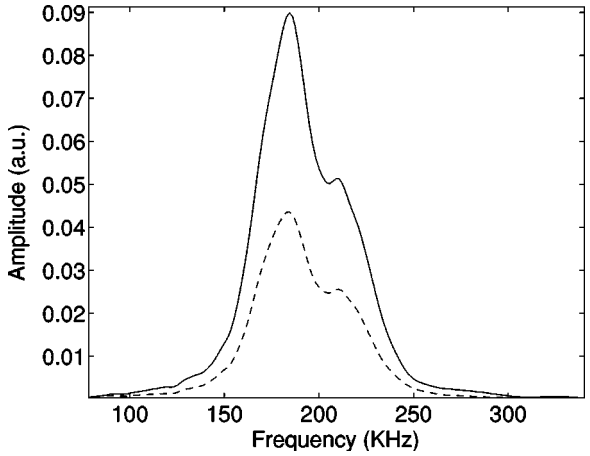

FIG. 9. Spectrum of experimental incident signal (solid line) and of experimental reflected signal (dashed line) for $\theta=25°$.

$$\alpha_\infty=\frac{\left(\frac{(1-r2)(1+r1)\cos\theta_2}{(1+r2)(1-r1)\cos\theta 1}\right)^2\sin^2\theta_1-\sin^2\theta_2}{\left(\frac{(1-r2)(1+r1)\cos\theta_2}{(1+r2)(1-r1)\cos\theta 1}\right)^2-1}. \tag{20}$$

Knowing the value of tortuosity, we deduce the expression of the porosity function for $\theta 1$ and $r1$ by the expression

$$\phi=\frac{\alpha_\infty(1-r1)\cos\theta_1}{(1+r1)\sqrt{\alpha_\infty-\sin^2\theta_1}}, \tag{21}$$

or expression of the porosity function for θ_2 and $r2$:

$$\phi=\frac{\alpha_\infty(1-r2)\cos\theta_2}{(1+r2)\sqrt{\alpha_\infty-\sin^2\theta_2}}. \tag{22}$$

In application of this model, some numerical simulations are compared with experimental results. Experiments are performed in air using two broadband Ultran NCT202 trans-

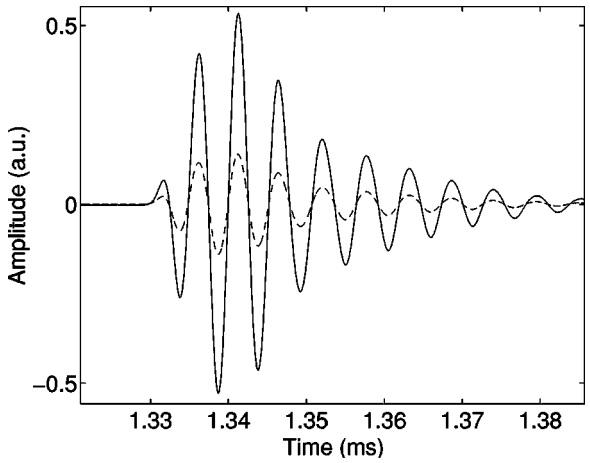

FIG. 10. Experimental incident signal (solid line) and experimental reflected signal (dashed line) for $\theta=66°$.

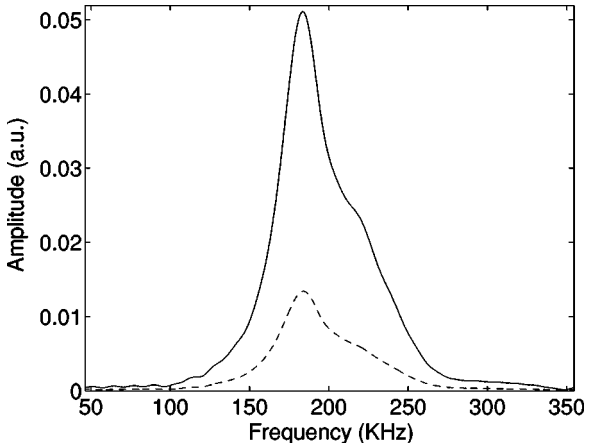

FIG. 11. Spectrum of experimental incident signal (solid line) and of experimental reflected signal (dashed line) for $\theta=66°$.

ducers with a central frequency of 190 kHz in air and a bandwidth of 6 dB extending from 150 to 230 kHz. 400 V pulses are provided by a 5052PR Panametrics pulser/receiver. The signals received are amplified to 90 dB and filtered above 1 MHz to avoid high frequency noise. Electronic interference is removed by 1000 acquisition averages. The experimental setup is showed in Fig. 6. Signal duration is important as its spectrum must verify the condition of high frequency approximation referred to in the previous section.

Take a sample of random packings of glass beads, M2, with the following parameters: resistivity $\sigma=12\,300$ $\mathrm{N\,m^{-4}\,s}$, diameter 0.1 ± 0.02 mm, $\Lambda=90$ μm, and $\Lambda'=180$ μm. Figure 7 shows the sample of random packings of glass beads M2.

Figure 8 shows the incident signal generated by the transducer (solid line) and the signal reflected by the sample M2 (dashed line) at an angle of incidence $\theta=25°$. Figure 9 shows their spectra. From the spectra of the two signals, the reader can see that they have the same bandwidths, which means there is no dispersion.

Figure 10 shows the incident signal generated by the transducer (solid line) and the signal reflected by the sample M2 (dashed line) for an angle of incidence $\theta=66°$. Figure 11 shows their spectra. Here, again, we can conclude from the two spectra that there is no dispersion. This concurs with the theory below which predicts that the wave reflected from the first interface $x=0$ is measured and simply attenuated by the factor

$$(\alpha_\infty \cos\theta-\phi\sqrt{\alpha_\infty-\sin^2\theta})/(\alpha_\infty \cos\theta+\phi\sqrt{\alpha_\infty-\sin^2\theta}).$$

Tables I and II give the tortuosity and porosity calculated using Eqs. (20) and (21) for each pair of the incidence angles θ_1 and θ_2. It can be seen in Tables I and II that the calculated values of the porosity and tortuosity are nearly constant. Two pairs of angle 25.3°–27.5° and 27.5°–30° give unacceptable values of the tortuosity. This could be caused by the great sensitivity of the tortuosity to small variations of the incidence angle, and so these results can be explained by experimental errors. The average tortuosity obtained from these measurements is $\alpha_\infty=1.87$ and the average porosity obtained is $\phi=0.44$.

TABLE I. Values of the tortuosity and porosity calculated for each pair of incidence angles θ_1 and θ_2.

Angle of incidence θ_1/θ_2 (deg)	Tortuosity	Porosity
0/25.3	1.817	0.435
0/27.5	1.893	0.444
0/30	1.815	0.435
0/41.6	1.828	0.436
0/44	1.828	0.436
0/57.2	1.890	0.443
0/66.6	1.886	0.443
25.3/27.5	2.45	0.498
25.3/30	1.81	0.434
25.3/41.6	1.83	0.437
25.3/44	1.833	0.436
25.3/57.2	1.906	0.444
25.3/66.6	1.897	0.443
27.5/30	1.51	0.404

TABLE II. Values of the tortuosity and porosity calculated for each pair of incidence angles θ_1 and θ_2.

Angle of incidence θ_1/θ_2 (deg)	Tortuosity	Porosity
27.5/41.6	1.784	0.433
27.5/44	1.792	0.433
27.5/57.2	1.889	0.443
27.5/66.6	1.884	0.443
30/41.6	1.84	0.437
30/44	1.838	0.437
30/57.2	1.917	0.445
30/66.6	1.903	0.443
41.6/44	1.829	0.436
41.6/57.2	1.94	0.446
41.6/66.6	1.924	0.444
44/57.2	1.983	0.448
44/66.6	1.932	0.444
57.2/66.6	1.885	0.443

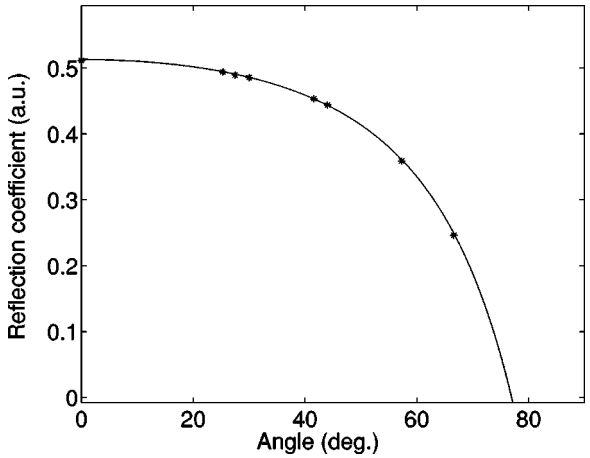

FIG. 12. Simulation of variation of the reflection coefficient (solid line) with the angle of incidence θ and experimental data of the reflection coefficient (star).

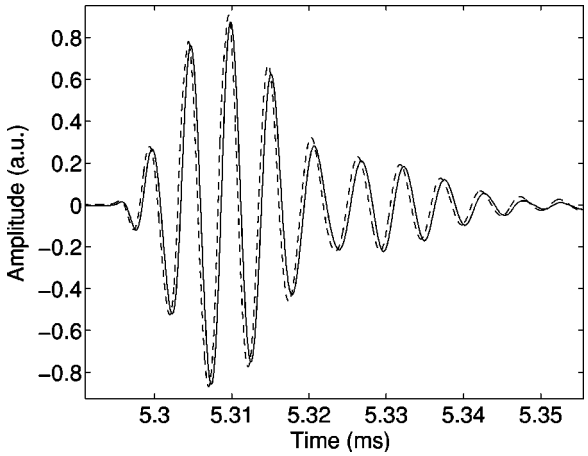

FIG. 13. Comparison between experimental reflected signal (solid line) and simulated reflected signal (dashed line) for $\theta=25°$.

Figure 12 shows the experimental data for the reflection coefficient at different angles of incidence θ, and simulation of the variation in reflection coefficient with the angle of incidence θ at a tortuosity of $\alpha_\infty=1.7$ and porosity $\phi=0.44$. The porosity of the glass bead, M2, given by the porosimeter[21] is $\phi=0.4\pm0.1$, and the tortuosity given by the classical method[7,8,23,24] is $\alpha_\infty=1.9\pm0.2$, so it can be seen that the slight difference between the porosity and tortuosity measured using this method and the other classical methods. Figure 13 shows the comparison between the simulated reflected signal at the first interface calculated for $\alpha_\infty=1.87$ and $\phi=0.44$, and the experimental reflected signal for $\theta=25°$. Figure 14 shows the same comparison for $\theta=66°$.

The difference between the simulated reflected signal and experimental reflected signal is slight, leading to the conclusion that the values of tortuosity and porosity obtained are good. To progress in this area, future work must improve experimental methods and inversion algorithms.

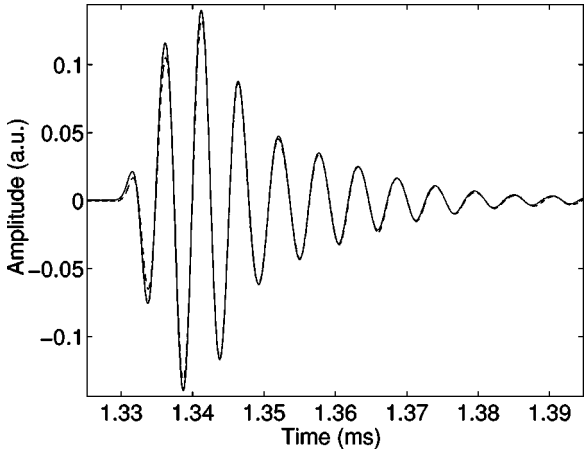

FIG. 14. Comparison between experimental reflected signal (solid line) and simulated reflected signal (dashed line) for $\theta=66°$.

APPENDIX: GREEN FUNCTION OF THE MEDIUM

The Green function of the propagation Eq. (6) is given in Ref. 7 by

$$F(t,k)=\begin{cases}0 & \text{if } 0\leqslant t\leqslant k\\ \Xi(t)+\Delta\displaystyle\int_0^{t-k}h(t,\xi)d\xi, & \text{if } t\geqslant k,\end{cases}$$

with

$$\Xi(t)=\frac{b'}{4\sqrt{\pi}}\frac{k}{(t-k)^{3/2}}\exp\left(-\frac{b'^2k^2}{16(t-k)}\right),$$

where $h(\tau,\xi)$ has the following form:

$$h(\xi,\tau)=-\frac{1}{4\pi^{3/2}}\frac{1}{\sqrt{(\tau-\xi)^2-k^2}}\frac{1}{\xi^{3/2}}\times\int_{-1}^{1}\exp\left(-\frac{\chi(\mu,\tau,\xi)}{2}\right)[\chi(\mu,\tau,\xi)-1]\frac{\mu d\mu}{\sqrt{1-\mu^2}},$$

and where

$$\chi(\mu,\tau,\xi)=[\Delta\mu\sqrt{(\tau-\xi)^2-k^2}+b'(\tau-\xi)]^2/8\xi,$$

$$b'=Bc_0^2\sqrt{\pi},\quad c'=C.c_0^2$$

and

$$\Delta=b'^2-4c',$$

when $k\to\infty$, Ξ and $h(\xi,\tau)$ tends to zero, then the Green function $F(t,k)$ also tends to zero.

[1] K. Attenborough, J. Acoust. Soc. Am. **81**, 93 (1987).
[2] *Disorder and Granular Media*, edited by D. Bideau and A. Hansen (North-Holland, New York, 1993).
[3] K. Attenborough, Acta Acustica **1**, 213 (1993).
[4] D. L Lafarge, P. Lemarnier, J. F. Allard, and V. Tarnow, J. Acoust. Soc. Am. **102**, 1995 (1997).
[5] J. F. Allard, M. Henry, and J. Tizianel, J. Acoust. Soc. Am. **107**, 2004 (1998).
[6] Z. E. A. Fellah and C. Depollier, J. Acoust. Soc. Am. **107**, 683 (2000).
[7] Z. E. A. Fellah, C. Depollier, and M. Fellah, J. Sound Vib. **244**, 359 (2001).
[8] Z. E. A. Fellah, C. Depollier, and M. Fellah, Acta Acustica **88**, 34 (2002).
[9] D. L. Johnson, J. Koplik, and R. Dashen, J. Fluid Mech. **176**, 379 (1987).
[10] J. F. Allard, *Propagation of Sound in Porous Media: Modeling Sound Absorbing Materials* (Chapman and Hall, London, 1993).
[11] M. A. Biot, J. Acoust. Soc. Am. **28**, 168 (1956).
[12] M. A. Biot, J. Acoust. Soc. Am. **28**, 179 (1956).
[13] K. Attenborough, Phys. Lett. **82A**, 179 (1982).
[14] C. Zwikker and C. W. Kosten, *Sound Absorbing Materials* (Elsevier, New York, 1949).
[15] Y. Champoux and J. F. Allard, J. Acoust. Soc. Am. **91**, 3346 (1992).
[16] L. L. Beranek, J. Acoust. Soc. Am. **13**, 248 (1942).
[17] R. W. Leonard, J. Acoust. Soc. Am. **20**, 39 (1948).
[18] E. Guyon, L. Oger, and T. J. Plona, J. Phys. D **20**, 1637 (1987).
[19] D. L. Johnson, T. J. Plona, C. Scala, F. Psierb, and H. Kojima, Phys. Rev. Lett. **49**, 1840 (1982).
[20] J. Van Brakel, S. Modry, and M. Svata, Powder Technol. **29**, 1 (1981).
[21] Y. Champoux, M. R. Stinson, and G. A. Daigle, J. Acoust. Soc. Am. **89**, 910 (1991).
[22] S. G. Samko, A. A. Kilbas, and O. I. Marichev, *Fractional Integrals and Derivatives: Theory and Applications* (Gordon and Breach Science, Amsterdam, 1993).
[23] P. Leclaire, L. Kelders, W. Lauriks, N. R. Brown, M. Melon, and B. Castagnède, J. Appl. Phys. **80**, 2009 (1996).
[24] N. Brown, M. Melon, V. Montembault, B. Castagnède, W. Lauriks, and P. Leclaire, C. R. Acad. Sci. Paris **322**, Series IIb, Acoustics, 121 (1996).